IET Microwaves, Antennas & Propagation

Research Article

IET Journals
The Institution of Engineering and Technology

Multiple-input multiple-output beam-space for high-speed wireless communication in underground mine

ISSN 1751-8725
Received on 14th July 2014
Revised on 6th August 2015
Accepted on 27th August 2015
doi: 10.1049/iet-map.2014.0464
www.ietdl.org

Mohamad Ghaddar[1], Mourad Nedil[1] ✉, Ismail Ben Mabrouk[1], Larbi Talbi[2]

[1]*School of Engineering, University of Quebec (UQAT), Val d'Or, Quebec, Canada*
[2]*Department of Computer Science and Engineering, University of Quebec (UQO), Gatineau, Quebec, Canada*
✉ *E-mail: Mourad.Nedil@uqat.ca*

Abstract: This study presents a new low-cost multiple-input multiple-output (MIMO) beam-pace technique to increase the overall link capacity of wireless MIMO communications systems in scatter-rich underground mines. This technique is based on generating multiple orthogonal beams for data spatial multiplexing using conformal cylindrical-shape patch arrays. Hence, this study is intended to reveal interests towards the use of conformal MIMO systems for underground mine communications. Two separate 4×4 MIMO measurement campaigns are performed and then investigated in a comparative way; the first uses conformal microstrip patch arrays (CMPA), while the second uses conventional planar microstrip patch arrays (PMPA). Based on sweeping-frequency technique (2.35–2.55) GHz, the channel performance is characterised in terms of path loss, fading distribution, capacity and RMS time dispersion parameters. Whether under a line of sight (LOS) or a non-LOS (NLOS) condition, the extracted results confirm the performance priority of CMPA for underground mines communications as they further enhance the propagation characteristics and the capacity gain of the channel; under NLOS, a maximal capacity of 12.95 bits/s/Hz is achieved compared to 9.6 bits/s/Hz obtained using PMPA. For LOS and NLOS cases, maximal capacity boosts of up to 0.43 and 3.35 bits/s/Hz are achieved over PMPA, respectively.

1 Introduction

The mining industry is one of the most important economic sectors for global prosperity [1]. In fact, the efficient exploitation of mineral resources for mining industry requires reliable and errorless communication systems that maximise miners' safety and reduce the operational costs [2]. Establishing a reliable wireless link in underground mines is a challenging task as their characterisation requires dealing with confined, dense and complex geological structure environments containing extremely rough and irregular surfaces. Thus, underground mines have been gaining more research interests to describe their hostile propagation characteristics accurately [2].

Currently, most underground mines are equipped with legacy communications systems such as the leaky feeders which suffer from the limited coverage and require a line of sight (LOS) path [3]. Multiple-input multiple-output (MIMO) systems are well-proven for both LOS and non-LOS (NLOS) indoor wireless communications as they exploit efficiently the channel's multipath and turn it into a key feature for increasing the data throughput speed [4, 5]. In the 2.4 GHz band, several standards have appeared for confined indoor wireless local area networks communications, among them is the IEEE 802.11n which allows up to four spatial streams and offers up to 600 Mbps [6]. The indoor proven MIMO technologies do not necessarily succeed in underground mines, due to the difference in their structural nature. Thus, the prosperity of indoor MIMO technologies has urged several research activities towards the exploration of MIMO systems in the 2.4 GHz band as alternatives to overcome the limitation of current communications in such environments [3, 7–9]. To date, an enormous expansion of research activities has occurred to improve underground MIMO channel performances. These techniques deal with the effects of polarisation [10, 11], antenna spacing [12], orthogonal frequency division multiplexing [13] and antenna sub-array formation that requires variable radio-frequency (RF) phase shifters and variable gain-linear amplifiers [14]. However, all these MIMO techniques exhibit several drawbacks in terms of hardware complexity, size, and cost-effectiveness. Beam-space MIMO (BS-MIMO) smart systems have been recently proposed by several research activities as an alternative solution to address the shortcomings of those conventional MIMO systems. In this approach, instead of sending symbol streams directly on the array elements as in the traditional case, these symbols are mapped directly onto a selected set of radiation angles of departure that constitute an orthogonal basis in the beam-space domain [15, 16]. Indeed, a physical beam steering is considered impractical and requires complex algorithms [17]. Thus, the first step towards facilitating BS-MIMO transmission has been made by means of an electronic steerable passive array radiator antenna as proposed in [17].

In this paper, the proposed MIMO-BS system for underground mine communications is based on a switched beam conformal array antenna. This technique generates orthogonal multiple-beams and enhances the decorrelation of MIMO sub-channels and hence, boosts the channel capacity. Furthermore, the conformal-shaped array, (i.e. cylindrical) allows the orientation of the radiation directivity towards the desired angles, and thus, reduces the required amount of transmitted power and prevents the signal's blockage when obstacles are present in the channel. The integration of multi-beams antenna technology in MIMO systems is expected to significantly improve the capacity of rich-multipath underground mines, especially under NLOS.

Therefore, the main purpose of this study is to investigate the constructive effects of conformal microstrip patch arrays (CMPA) antennas on the channel propagation characteristics. To yield a clear insight into the performance of CMPA technique, it is then compared to the conventional planar microstrip patch arrays (PMPA). Hence, under both LOS and NLOS scenarios, two separate MIMO propagation measurement campaigns are carried out using (a) 4×4 PMPA and then (b) 4×4 CMPA.

The data throughput speed is evaluated by means of the channel capacity (in bits/s/Hz) which depends on the statistical propagation characteristics such as the path loss (PL) and root mean square

(RMS) time delays. In other words, the more relevant channel statistical parameters are expected to yield higher data transmission rates.

The remaining of the paper is organised as follows: Section 2 introduces the channel's sounder hardware setup. Section 3 describes the considered environment and the measurement procedure. Then Section 4 gives details about the statistical analysis of the experimental data and presents the obtained experimental results. Finally, Section 5 is reserved for the conclusion.

2 Measurement setup and methodology

2.1 Hardware setup

Using the sweeping-frequency technique, the variations of 4001complex tones were measured across 2.35–2.55 GHz band. To compensate for the attenuation in feeding coaxial cables, a power amplifier (PA) and a low noise amplifier (LNA) are used at T_X and R_X sides, respectively, each with a gain of 30 dB. More details about the measurement system's setup are provided in [7] (Fig. 1). As a result of a frequency resolution of 50 kHz (approximately), a maximum resolvable delay of 20,000 ns is recorded. In other words, the measurement system is capable of catching multipath components that arrive within 20,000 ns or a maximum observable distance of 600 m. The frequency span of 200 MHz provides a temporal resolution of 5 ns or a spatial resolution of 1.5 m. Hence, the channel's sounder assures an adequate temporal resolution of multipath components that arrive at the receiver within few nanoseconds of the interval. Finally, the system includes two identical antenna arrays; each was equipped with an RF switch (Pulsar, SW2AD-22). Each of the 16 MIMO channels $\{h_{11}, h_{12}, \ldots, h_{R_X T_X}\}$ was measured sequentially using the switches assuming a quasi-static channel.

2.2 MIMO arrays design

The measurements were performed using the MIMO patch arrays presented in Fig. 2, their technical specifications are presented in Table 1.

The spacing between elements is set to 6 cm which corresponds to one-half average wavelength ($\lambda/2$). This range ensures uncorrelated and independent channels which result in a higher channel capacity [9]. Two different antenna array configurations have been considered during the measurements. The first one is the planar microstrip patch antenna array MIMO configuration (PMPA), it was designed and fabricated in the LRTCS using HFSS software tool (Ansoft). For the second MIMO configuration, i.e. the conformal antenna array (CMPA), the multiple orthogonal beams

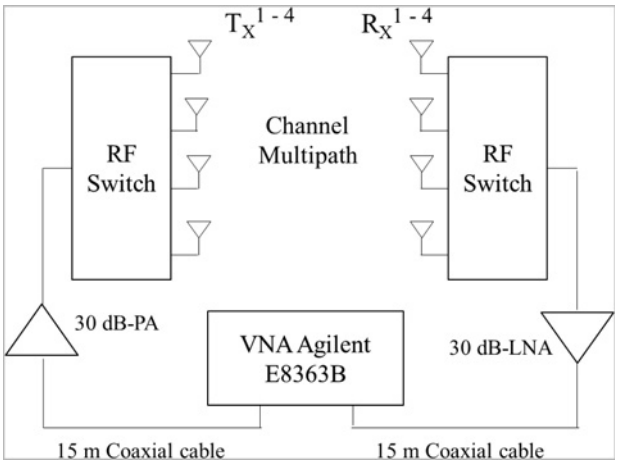

Fig. 1 *Schematic diagram of the channel measurement setup*

were generated by setting the angle between adjacent elements to 30° (Figs. 2*c* and *d*). It is worth to mentioning that 30° angles were obtained by rolling up the flexible substrate of PMPA over a cylinder having a radius '*r*', calculated as (a/θ), where '*a*' is the arc length ($\lambda/2$) and θ is the angle in radians. The reason behind the latter structure was to extend the signal coverage over the entire azimuth angle facing the antenna array. This configuration overcomes the ambiguity of multipath directions of arrival (DoA) and enhances their gains in all directions [18, 19]. Therefore, CMPA structure is expected to gather a large amount of multipath.

3 Measurement site and procedure

3.1 Site description

The measurements were carried out in a real underground gold mine as shown in Fig. 3. More details about the mine are provided in [7, 8]. This former gold mine is located in approximately 530 km north-west of Ottawa, Canada. Presently, it is operated by MMSL CANMET (Mining and Mineral Sciences Laboratories-Canadian Center for Minerals and Energy Technology) for the purpose of experimental research, training and testing. Thus, the reported results of [7] have been given a particular attention as they were obtained in the undertaken gallery, but with 2×2 MIMO patch arrays similar to the presented PMPA.

At 40 m below the ground level, the L-shaped gallery stretches over a length of 75 m with a width and a height of 3.4 and 4.6 m, respectively. The ground is rather undulating and sparse with a huge amount of dust. The gallery sidewalls are structured from soil and rocks. They have a significant roughness, their surfaces irregularities vary at an average rate of 25 cm. As seen in Fig. 3, a hanging transparent drape takes a place behind T_X. It is made of plastic rags and has no effects on the propagating signal.

3.2 Measurement procedure

Each measurement scenario was performed using two identical T_X and R_X antenna arrays, i.e. either PMPA or CMPA. During all measurements, T_X and R_X antenna arrays were maintained at a height of 1.4 m, almost at the central line of the mining gallery to efficiently capture the effects of all surrounding surfaces. The channel was kept stationary by ensuring that miners were not present in the surrounding environment. The small-scale measurements were obtained by arranging R_X on a 7×7 ($N_x \times N_y$) points square grid. The spacing between two adjacent points of the grid was chosen to be a one half-wavelength ($\Delta_x = 6$ cm) to obtain approximately uncorrelated samples. Hence, at each position along the gallery, T_X was moved mechanically within the grid where 49 measurement snapshots were recorded. Both LOS and NLOS scenarios were investigated as illustrated in Fig. 4.

(i) *LOS scenario*: In this scenario, T_X was remained stationary all the time. The large-scale measurements were performed while moving R_X away from T_X on the central line of the galley from A to B (2–30 m), with an increment of 2 m (Fig. 4).
(ii) *NLOS scenario*: This measurement campaign was similar to the previous one. The initial position of R_X was set at point A (Fig. 4) to guarantee the blockage of the LOS between both ends, and then R_X was moved towards its final position (point B) with an increment of 2 m, as preceded in the previous scenario. For a deeper experimental analysis, it would have been more interesting to carry measurements at larger T_X–R_X distances, however, the sounding equipment were limited to a maximum range of 30 m. Such range ensures relevant channel statistical parameters and provides adequate information about the channel characteristics in the 2.4 GHz band [7–9, 20].

For each R_X position on the grid, the channel transfer function (CTF) was measured seven times ($N_S = 7$ snapshots) to reduce the

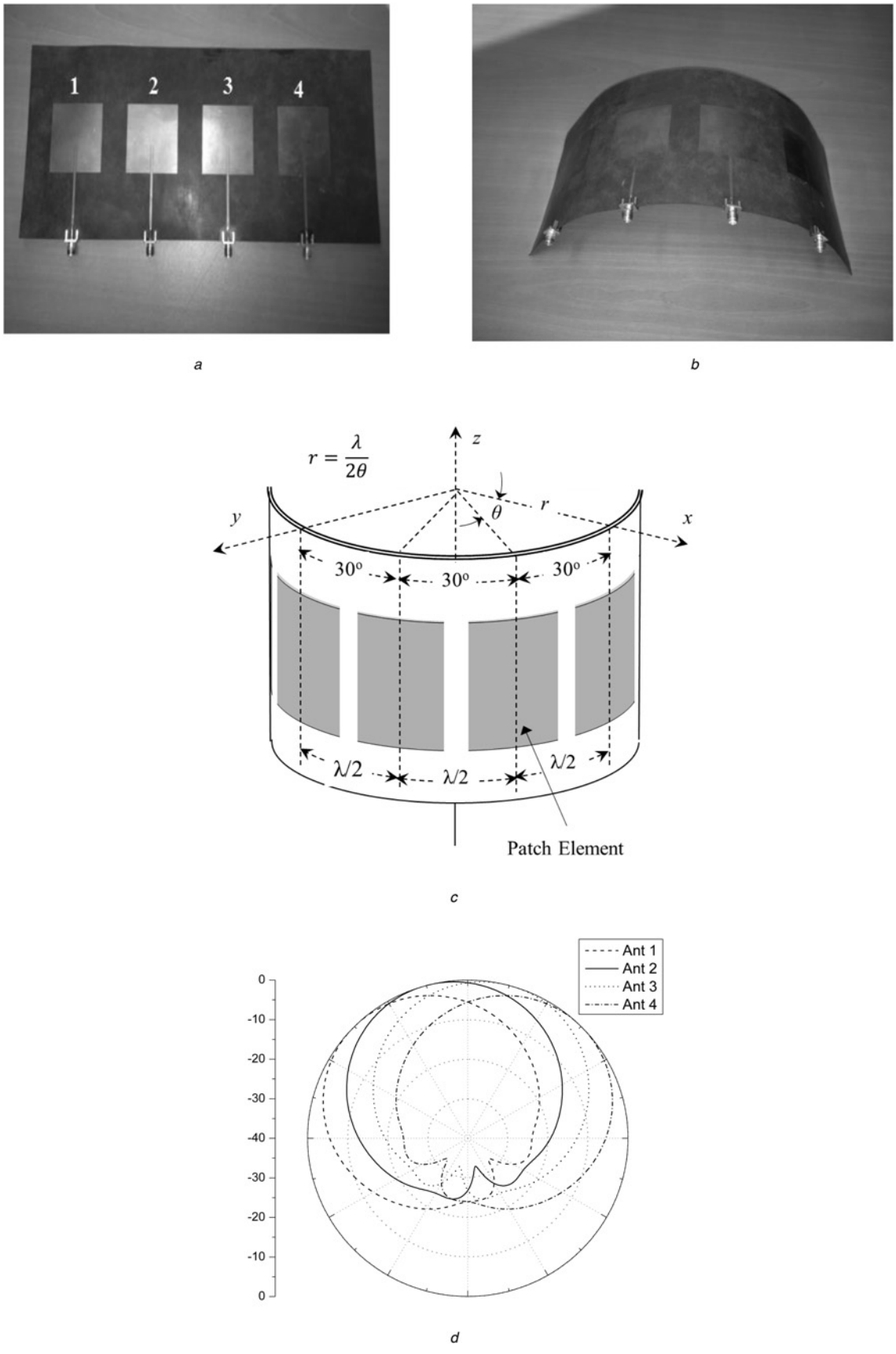

Fig. 2 *4-Elements microstrip patch antenna arrays PMPA and CMPA*

a Conventional planar shape (PMPA)
b Conformal shape (CMPA)
c Geometrical shape of CMPA
d Simulated radiation patterns for conformal patch antenna

IET Microw. Antennas Propag., 2016, Vol. 10, Iss. 1, pp. 8–15

Table 1 Arrays microstrip patch elements technical specifications

Polarisation	Vertical
beam's elevation cut	71.3°
azimuth cut	92.4°
gain	7 dBi
frequency range	2.35–2.55 GHz

effects of the random noise on the experimental data, and then stored in the vector network analyser (VNA) memory. The received $N_S \times N_x \times N_y$ ($7 \times 7 \times 7 = 343$) snapshots are then averaged for each R_X location (d) throughout the gallery to yield the final measured CTF as

$$\boldsymbol{G}_{f,d} = \frac{1}{N_s}\frac{1}{N_x N_y}\left\{\sum_{i=1}^{N_s}\sum_{j=1}^{N_x N_y} A(f,x,y,s,d)\, e^{\theta(f,x,y,s,d)}\right\}$$
$$x \in \{1,2\ldots,N_x\},\ y \in \{1,2\ldots,N_y\} \quad \text{and} \quad s \in \{1,2\ldots,N_s\} \tag{1}$$

where $A(x, y, s, f)$ and $\theta(x, y, s, f)$ are the measured magnitude and phase response at of the snapshot s at frequency f and position on the grid (x, y), respectively. Following the approach in [7], the three-dimensional (3D) MIMO channel matrix $\boldsymbol{h}_f^{N_R \times N_T \times N_f}$ is formed by collating the transfer functions of all 16 sub-channels (G_f), where N_R, N_T and N_f are the number of transmit array elements, receive array elements, and discrete frequency components, respectively.

4 Analysis and measurement results

4.1 PL distance law (gradient)

The small-scale measurements were performed by averaging all ($49 \times 7 = 343$) CTFs, thus, the average of such large amount of data ensures the reliability of the obtained statistical results. For each R_X position, all obtained sub-channels are then averaged to yield the final channel CTF

$$\mathcal{H}_{f,d} = \frac{1}{N_R N_T}\left\{\sum_{i=1}^{N_R N_T} \boldsymbol{h}_f^{N_R \times N_T}\right\} \tag{2}$$

The average PL was estimated over all of the amplitudes of the measured CTF for each T_X–R_X separation distance d. We stress that the averaging was done on a linear scale (not in decibels) as

$$\mathrm{PL}_{\mathrm{dB}}(d) = 10\mathrm{Log}10\{[\varepsilon(|\mathcal{H}_{f,d}|)]^2\} \tag{3}$$

where $\varepsilon()$ denotes the expectation operator over all the CTF frequency tones. The PL at any location in the gallery can be described by a random lognormal (in dB) distribution as [18]

$$\overline{PL}_{\mathrm{dB}}(d) = \overline{PL}_{\mathrm{dB}}(d_o) + 10\, n\, \mathrm{Log}_{10}\left(\frac{d}{d_o}\right) + S(d) \tag{4}$$

where $\overline{\mathrm{PL}}_{\mathrm{dB}}(d_o)$ is the averaged PL in decibels at a reference distance d_o from the transmitter, in our case $d_o = 1$ m, n is the PL exponent which is a measure of decay in the received power with the distance according to $1/d^n$. S denotes the shadowing fading parameter that varies from one location to another [21]. Fig. 5 shows scatter plots of the PL (dB) versus distance logarithmic scale and the minimised mean squared error (MMSE) fitted lines for both PMPA and CMPA MIMO configurations. Such linear fit serves to determine the PL exponent and the shadowing level.

Results of Table 2 indicate that under LOS scenario, the PL exponents of both MIMO configurations are almost equal with a very slight difference of 0.11. They are found to be smaller than the free space exponent ($n = 2$), this is due to the underground gallery structure which guides the wave. All multipath aggregate and contribute in enhancing the received signal.

However, under NLOS scenario, MIMO-CMPA configuration exhibits a further suppression in the PL exponent by 1.24 as compared to MIMO-PMPA. Indeed, the four CMPA beams are oriented in different directions to cover the entire azimuth angle within the area facing directly the antenna, contrary to what happens for PMPA, where the all the array gain is oriented in the same direction.

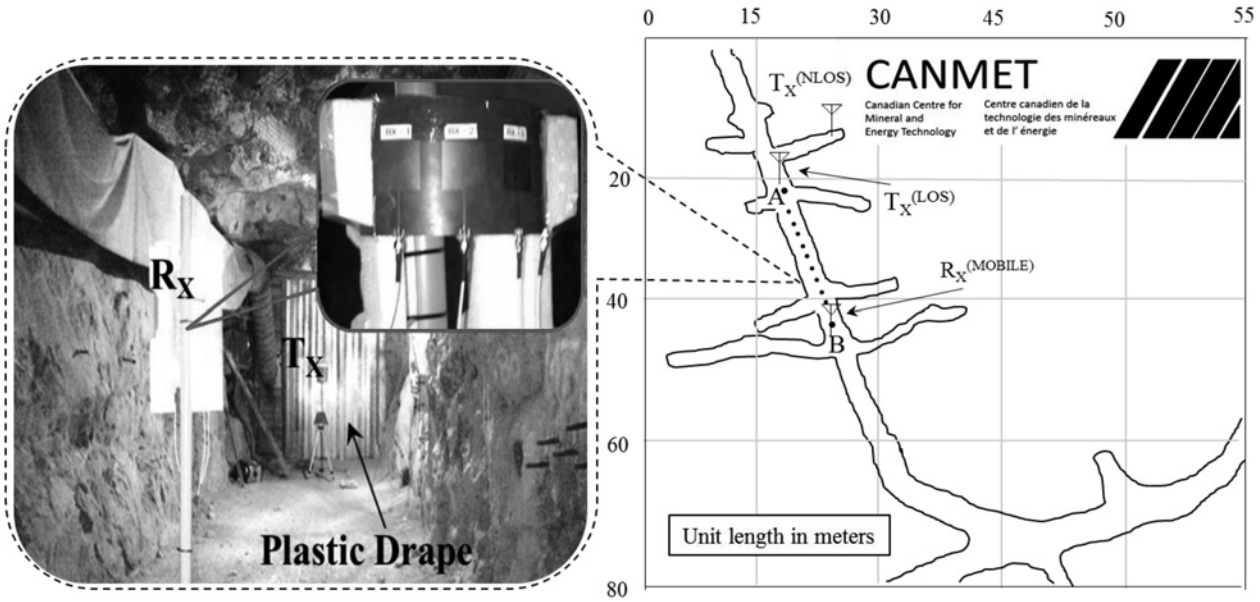

Fig. 3 *Photograph and a map of the CANMET gallery and T_X–R_X locations*

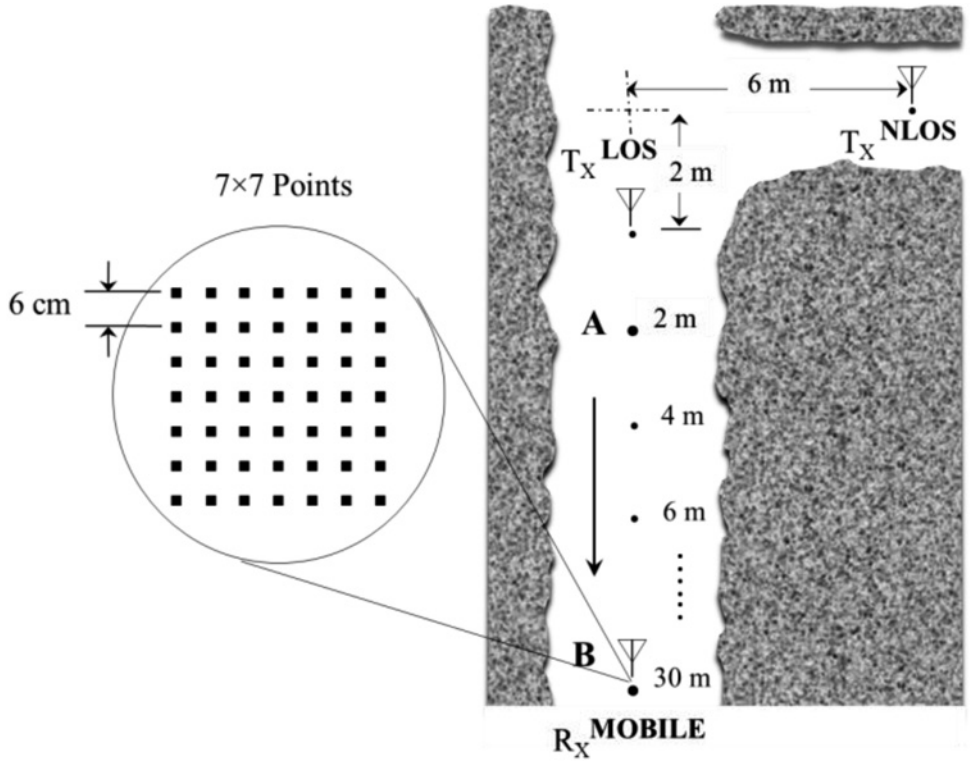

Fig. 4 *Illustrative top view of the considered LOS/NLOS measurement scenarios*

4.2 Fading distributions and shadowing effects

The cumulative distribution functions (CDFs) of the deviation between the fitted and the measured data are plotted versus the normal CDF (Fig. 6). These curves show that the shadow fading of underground mine environments are lognormally distributed.

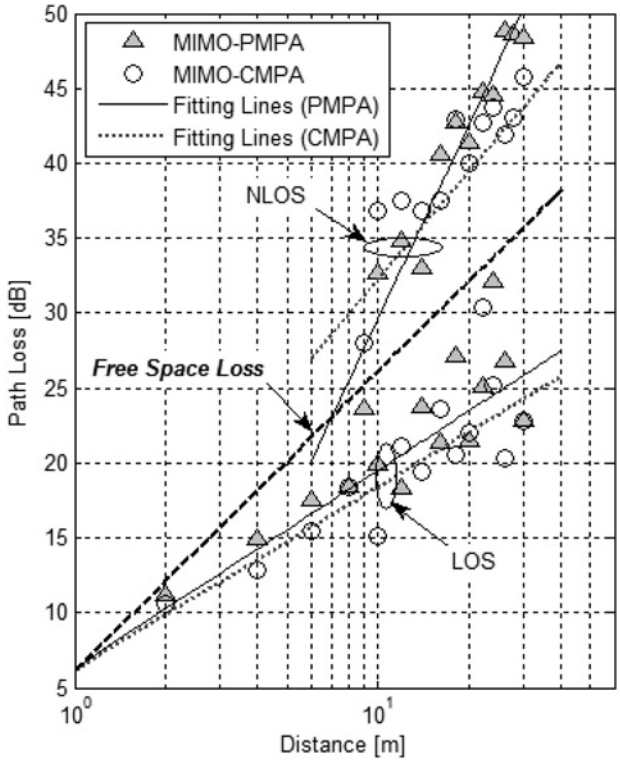

Fig. 5 *Measured path loss versus T_X–R_X separation distance*

Actually, the variations in the surrounding environment cause the incident direct wave to vary with respect to the sum of heavy multipath in the channel. Such variation causes random fluctuations in the mean signal power over large distances.

This manifestation is known as the shadow fading phenomenon and has been reported by many underground measurements [20, 22]. The shadow fading parameter S of (4) is lognormally distributed around its mean value, this zero-mean Gaussian-distributed random variable is expressed in dB. The standard deviation of S of both MIMO configurations for LOS and NLOS cases are given in Table 3. Under LOS, the parameter σ_S obtained using PMPA is found to agree with that obtained in [7]. The large values of σ_S emphasise the high power variation in underground mine environments. Thus, as a result of the heavy amount of multipath, CMPA subjects to a higher signal variation with respect to its mean as compared to PMPA case.

4.3 Time dispersion characteristics

The power delay profile (PDP) is referred as the squared magnitude of the channel's impulse response. Since the measurements are performed using the frequency sweep technique, the PDPs are obtained by applying the inverse discrete Fourier transform (IDFT) to the complex CTF of (1) measured at each R_X location (d) throughout the gallery. Mathematically, the PDP can be expressed as

$$\mathrm{PDP}_{t,d} = |\mathrm{IDFT}\{\boldsymbol{G}_{f,d}\}|^2 \tag{5}$$

Table 2 Statistics of the PL and the PL exponent (n)

Array type scenario	PMPA		CMPA	
	LOS	NLOS	LOS	NLOS
min., dB	11.2	23.6	10.5	28
max., dB	32.1	49.1	30.3	45.8
mean, dB	20.38	40.3	18.45	38.71
n	1.29	3.8	1.18	2.56

IET Microw. Antennas Propag., 2016, Vol. 10, Iss. 1, pp. 8–15

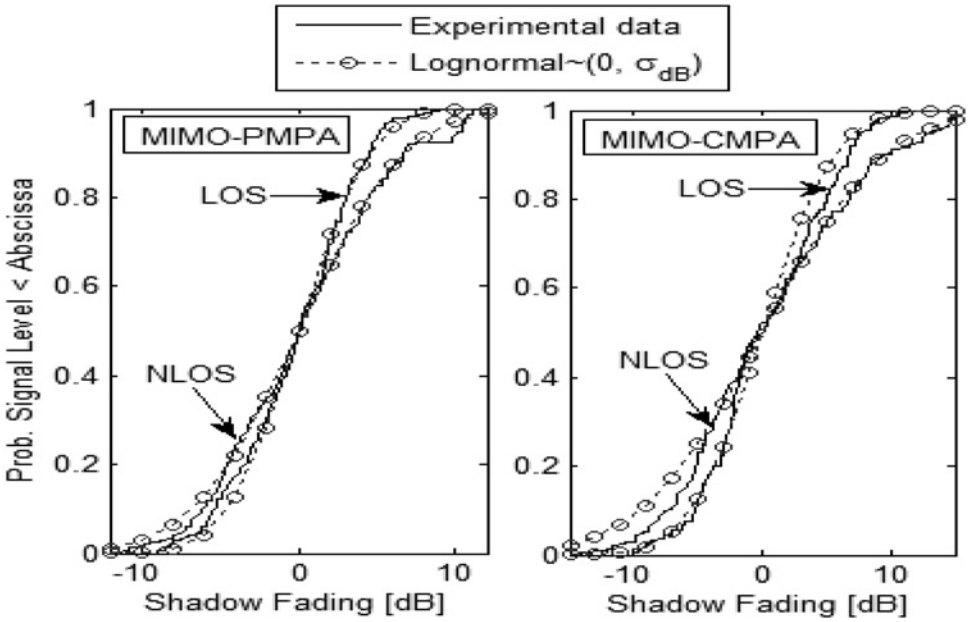

Fig. 6 *CDFs of shadowing fading fit for normal distribution*

Thus, for each R_X location ($N_R \times N_T$) PDPs are extracted. The mean excess delay (τ_m) and RMS delay spread (σ_τ) are computed from the corresponding PDP. The channel τ_m is the first moment of the PDP, corresponding to the centre of gravity of the profile and σ_τ is the square root of the second central moment of the PDP. The latter parameter is the most important as it gives an estimation of the amount of inter-symbol interference to be encountered in the channel; they are computed as [23]

$$\tau_m = \frac{\sum_k \alpha_k^2 \tau_k}{\sum_k \alpha_k^2}; \qquad \sigma_\tau = \sqrt{\frac{\sum_k \alpha_k^2 . \ (\tau_k - \tau_m)^2}{\sum_k \alpha_k^2}} \tag{6}$$

where a_k and τ_k are the amplitude and the delay of the kth path, respectively. To suppress the noise effects on the statistics of multipath arrival delays, σ_t are extracted under the threshold level considered in [7], i.e. 10 dB below the strongest multipath component, thus σ_t obtained under LOS scenarios will be fairly referred to those obtained [7]. For each R_X location (d), $N_R \times N_T$ values of σ_t delays are extracted from the corresponding measured PDPs. Fig. 7 shows the probability of R_X position for which σ_t are less than a specified value, i.e. the CDF. The statistical mean and standard deviation of the obtained channel time dispersive parameters τ_m and σ_t are shown in Table 4. In LOS case, the large statistical values of σ_τ emphasise that CMPA subjects to higher spatial variations as compared to PMPA, where more multipath rays contribute to the received signal. However, in NLOS gallery, CMPA behaviour is quite the opposite, implying that few strong multipath are taking a place. A further suppression of about 5.73 ns in the average σ_t is achieved using the CMPA configuration, thus, as compared to the conventional PMPA, the shorter delay imposes a lower equalisation design complexity to counter the erroneous bits and thus to increase the channel throughput speed. Under LOS, σ_τ obtained using PMPA are found to be comparable to those reported in [7].

Table 3 Lognormal fading distribution statistical parameters

Array type scenario	PMPA		CMPA	
	LOS	NLOS	LOS	NLOS
σ_S, dB	3.08	1.93	3.61	2.65

4.4 Channel capacity

The channel capacity (in bits/s/Hz) gives a clear insight into the throughput speed of MIMO links, basically, the MIMO system capacity depends on both, the multipath richness and the signal-to-noise ratio (SNR) of the channel. These two factors behave differently as the channel conditions vary from LOS to NLOS. Thus, channels multipath and SNR are usually not independent and some tradeoff should be practiced when normalising out the SNR [24]. To evaluate the multipath effect on the MIMO channel capacity, an SNR of 10 dB is assumed constant regardless the position of the receiver throughout the gallery. During the analysis of MIMO capacity, it is a common practice to normalise the channel $\boldsymbol{H}$-matrices of each channel realisation of ($\boldsymbol{h}_f^{\text{MIMO}}$) in (2) and at each R_X location before investigating the effects of the channel multipath as a parameter. The Frobenius coefficients matrix $\|\boldsymbol{H}\|_F$ and the normalised channel matrix $\boldsymbol{H}_n$ for each channel realisation are expressed as

$$\boldsymbol{H}_n = \boldsymbol{H}\sqrt{\frac{N_T N_R}{\boldsymbol{H}_F^2}} \quad \text{where } \boldsymbol{H}_F = \sqrt{\sum_{i=1}^{N_T}\sum_{j=1}^{N_R}\left|\boldsymbol{h}_{f(i,j)}^{\text{MIMO}}\right|^2} \tag{7}$$

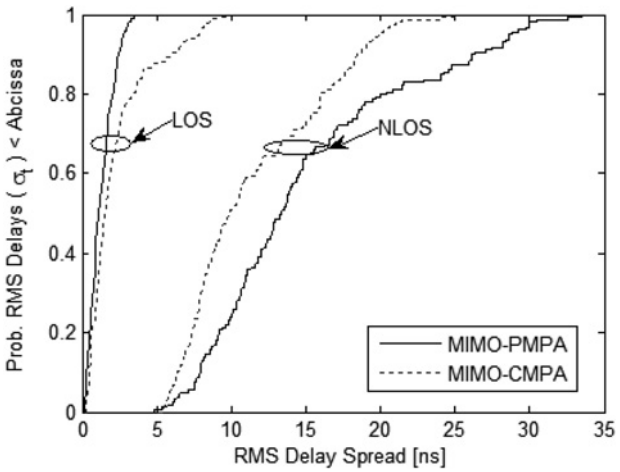

Fig. 7 *CDFs of the extracted RMS delay spreads*

Table 4 Statistical mean and standard deviation of σ_t and τ_m

Array type scenario		PMPA		CMPA	
		LOS	NLOS	LOS	NLOS
σ_t, ns	mean	1.38	15.6	2.08	11.47
	std.	1.09	6.21	1.16	4.7
τ_m, ns	mean	47.3	77.4	45.2	63.1
	std.	28.2	22.3	27.6	19.4

Table 5 Statistics of channel capacity [bits/s/Hz]

Array type scenario	PMPA		CMPA	
	LOS	NLOS	LOS	NLOS
min.	6.1	7.8	6.7	10.5
max.	8.3	9.6	8.73	12.95
mean	7.21	8.62	7.75	11.58
std.	0.69	0.58	0.67	0.85

Given the channel information at R_X for each frequency realisation, the channel capacity is estimated by Foshini and Gans as [25]

$$C = \log_2 \left\{ \det \left[\boldsymbol{I}_{N_R} + \frac{\text{SNR}}{N_T} \boldsymbol{H}_n \boldsymbol{H}_n^* \right] \right\} \text{bits/s/Hz} \quad (8)$$

where the superscript $(\cdot)^*$ denotes the Hermitian conjugate of the normalised channel matrix and $\boldsymbol{I}$ is the identity matrix. The channel capacity is estimated under the assumption of N_T individual sources with equal transmit power. Equation (8) gives insight into the logarithmic growth of MIMO systems capacity with respect to SNR assuming that the channel is perfectly known at the receiver. The maximum achievable error-free transmission (C_B) over the bandwidth of interest (B) at a location d, is given as [24]

$$C_B(d) = B \cdot C(d) \text{ bits/s} \quad (9)$$

Based on (8), the effects of CMPA on the channel capacity are investigated. As expected, higher capacities are obtained under NLOS scenario. This can be explained by the rich multipath environment which enhances the decorrelation between MIMO sub-channels and therefore, increases the channel capacity. Moreover, the results of Fig. 8 and Table 5 are clear evidences that MIMO-CMPA has provided better channel capacities for both scenarios, especially for the NLOS case. The mean shifts between these two configurations are 0.54 and 2.96 bits/s/Hz for LOS and NLOS, respectively.

Furthermore, the improvement in the link throughput speed in terms of the channel capacity offered by 4×4 MIMO over 2×2 MIMO link presented in the previous work under the same conditions [7] is noticeable, the capacity gain is almost doubled. The obtained results do not contradict the truth that the channel capacity increases in a linear tendency with the minimum number of T_X and R_X elements. Similar to the basis of this study, another MIMO measurement campaigns were carried out under LOS, but using 2×2 PMPA MIMO configurations [4]. At an SNR of 10 dB, the mean capacity achieved in our campaign is almost twice of that in [4].

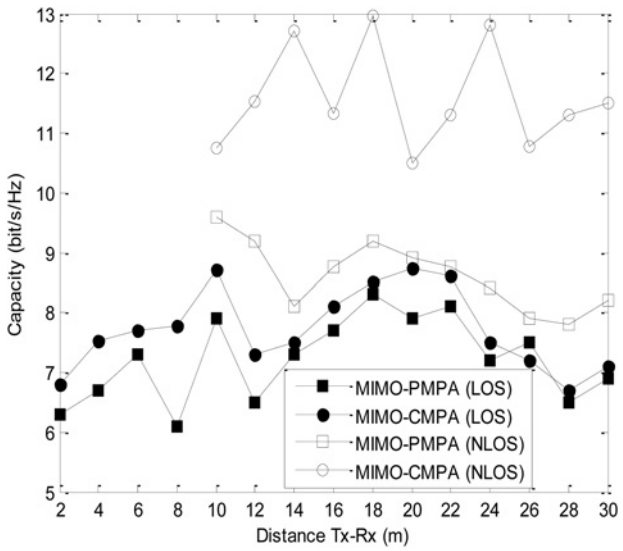

Fig. 8 *Estimated channel capacity versus T_X–R_X separation distance*

5 Conclusion

In this paper, the underground channel performance using a single RF chain MIMO-BS based on a conformal antenna array is discussed and analysed. The results show that the use of MIMO-BS systems in underground mines enhances considerably the channels performances, especially under NLOS scenarios. The proposed system shows: (i) a lower PL exponent, (ii) a further suppression of 14.3 and 4.13 ns in the average τ_m and σ_t delays, respectively and (iii) a higher maximal capacity of 12.95 bits/s/Hz compared to 9.6 bits/s/Hz obtained under NLOS using a conventional (PMPA) MIMO system. Furthermore, under NLOS, a larger channel coherence bandwidth (B) that is the reverse image of σ_t is offered using CMPA, according to (9), a higher link throughput speed in terms of the capacity is achieved under a shorter σ_t. Therefore, due to its low cost and simple design, the conformal structure is considered as a practical solution to maintain a robust wireless communication link in a complex geological structure environment such as the underground mine.

6 Acknowledgments

The authors gratefully acknowledge the reviewers for their comments toward the improvement of this paper. The financial support of National Sciences and Engineering council of Canada (NSERC) and the laboratory facilities provided by the LRTCS are also acknowledged.

7 References

1 Yarkan, S., Guzelgoz, S., Arslan, H., *et al.*: 'Underground mine communications: a survey', *IEEE Commun. Surv. Tutor.*, 2009, **11**, (3), pp. 125–142
2 Sun, Z., Akyildiz, I.F.: 'Channel modeling and analysis for wireless networks in underground mines and road tunnels', *IEEE Trans. Commun.*, 2010, **58**, (6), pp. 1758–1768
3 Forooshani, A., White, R., Michelson, G.: 'Effect of antenna array properties on multiple-input-multiple-output system performance in an underground mine', *IET Microw. Antennas Propag.*, 2013, **7**, (13), pp. 1035–8725
4 Valdesueiro, J.A., Izquierdo, B., Romeu, J.: 'On 2×2 MIMO observable capacity in subway tunnels at C-band: an experimental approach', *IEEE Antennas Propag. Lett.*, 2010, **9**, pp. 1099–1102
5 Lienard, M., Degauque, P., Baudet, J., *et al.*: 'Investigation on MIMO channels in subway tunnels', *IEEE J. Sel. Areas Commun.*, 2003, **21**, (3), pp. 332–339
6 IEEE Standard 802.11n-2009: Wireless LAN Medium Access Control and Physical Layer Specifications, Amendment 5: Enhancements for Higher Throughput
7 Ben Mabrouk, I., Talbi, L., Nedil, M., *et al.*: 'Effect of Antenna directivity on performance of MIMO systems in an underground gold mine', *IET Microw. Antennas Propag.*, 2012, **6**, (5), pp. 555–561
8 Ben Mabrouk, I., Talbi, L., Nedil, M., *et al.*: 'MIMO-UWB channel characterization within an underground mine gallery', *IEEE Antennas Propag. Trans.*, 2012, **60**, (10), pp. 4866–4874
9 Ben Mabrouk, I., Talbi, L., Nedil, M.: 'Performance evaluation of a MIMO system in underground mine gallery', *IEEE Antennas Wirel. Propag. Lett.*, 2012, **11**, pp. 830–833
10 Molina-Garcia-Pardo, J.M., Lienard, M., Simon, E., *et al.*: 'On the possibility of applying polarization diversity in tunnels'. Proc. MSWIM Conf., Tenerife, Spain, October 2009, pp. 392–395

11 Molina-Garcia-Pardo, J.M., Lienard, M., Degauque, P., *et al*.: 'MIMO channel capacity with polarization diversity in arched tunnels', *IEEE Antennas Wirel. Propag. Lett.*, 2009, **8**, pp. 1186–1189
12 Molina-Garcia-Pardo, J.M., Lienard, M., Degauque, P., *et al*.: 'On MIMO channel capacity in tunnels', *IEEE Trans. Antennas Propag.*, 2009, **57**, (11), pp. 3697–3701
13 Sanchis, C., Molina-Garcia-Pardo, J.M., Lienard, M., *et al*.: 'Performance evaluation of MIMO-OFDM in tunnels', *IEEE Antennas Propag. Lett.*, 2012, **11**, pp. 301–304
14 Theofilakos, P., Kanatas, A.G.: 'Capacity performance of adaptive receives antenna subarray formation for MIMO systems', *EURASIP J. Wirel. Commun. Netw.*, 2007, **2007**, pp. 1–12
15 Barousis, V.I., Kanatas, A.G., Kalis, A.: 'Beamspace-domain analysis of single-RF front-end MIMO systems', *IEEE Trans. Veh. Technol.*, 2011, **60**, (3), pp. 1195–1199
16 Alrabadi, O.N., Perrruisseau-Carrier, J., Kalis, A.: 'MIMO transmission using a single RF source: theory and antenna design', *IEEE Trans. Antennas Propag.*, 2012, **60**, (2), pp. 654–664
17 Gyoda, K., Ohira, T.: 'Design of electronically steerable passive array radiator (ESPAR) antennas'. Proc. IEEE Antennas Propagation Society Int. Symp., 2000, vol. 2, pp. 922–925
18 Sun, Z., Akyildiz, I.F., Haneke, G.P.: 'Capacity and outage analysis of MIMO and communication systems in underground tunnels', *IEEE Trans. Wirel. Commun.*, 2011, **10**, (11), pp. 3793–3803
19 Çaylar, S., Leblebicioglu, K., Dural, G.: 'Neural network method for direction of arrival estimation with uniform cylindrical microstrip patch array', *IET Microw. Antennas Propag.*, 2010, **4**, (2), pp. 153–161
20 Abdellah, C., Paul, F., Pierre, T.: 'Large-scale fading and time dispersion parameters of UWB channel in underground mines', *Int. J. Antennas Propag., Volume* 2008, Hindawi Publishing Corporation, Article ID 806326, 10 pp. doi: 10.1155/2008/806326
21 Cox, D.C., Murray, R., Norris, A.: '800 MHz attenuation measured in and around suburban houses', *AT&T Bell Lab. Tech. J.*, 1984, **673**, (6) pp. 921–954
22 Boutin, M., Benzakour, A., Despins, C., *et al*.: 'Radio wave characterization and modeling in underground mine tunnels', *IEEE Trans. Antennas Propag.*, 2008, **4**, (5), pp. 540–549
23 Rappaport, T.S.: 'Wireless communications: principle and practice' (Prentice-Hall, PTR, NJ, USA, 2002, 2nd edn.)
24 Telatar, I.E.: 'Capacity of multi-antenna Gaussian channels', *Eur. Trans. Telecommun.*, 1999, **10**, pp. 585–595
25 Foschini, G.J., Gans, M.J.: 'On limits of wireless communications in a fading environment when using multiple antennas', *Wirel. Pers. Commun.*, 1998, **6**, (3), pp. 311–335